Magnetoelastic distortion of multiferroic BiFeO3 in the canted antiferromagnetic state

T. Rõõm, J. Viirok, L. Peedu, U. Nagel, D. G. Farkas, D. Szaller, V. Kocsis, S. Bordács, István Kézsmárki, Dmytro Kamenskyi, H. Engelkamp, M. Ozerov, D. Smirnov, J. Krzystek, K. Thirunavukkuarasu, Y. Ozaki, Y. Tomioka, T. Ito, T. Datta, R. S. Fishman

Angaben zur Veröffentlichung / Publication details:

Rõõm, T., J. Viirok, L. Peedu, U. Nagel, D. G. Farkas, D. Szaller, V. Kocsis, et al. 2020. "Magnetoelastic distortion of multiferroic BiFeO3 in the canted antiferromagnetic state." *Physical Review B* 102 (21): 214410. https://doi.org/10.1103/physrevb.102.214410.

Magnetoelastic distortion of multiferroic $BiFeO_3$ in the canted antiferromagnetic state

T. Rõõm,[1,*] J. Viirok,[1] L. Peedu,[1] U. Nagel,[1] D. G. Farkas,[2,3] D. Szaller,[2,4] V. Kocsis,[2,5] S. Bordács,[2,6] I. Kézsmárki,[2,7] D. L. Kamenskyi,[8] H. Engelkamp,[8] M. Ozerov,[9] D. Smirnov,[9] J. Krzystek,[9] K. Thirunavukkuarasu,[10] Y. Ozaki,[11] Y. Tomioka,[11] T. Ito,[11] T. Datta,[12] and R. S. Fishman[13,†]

[1]*National Institute of Chemical Physics and Biophysics, Akadeemia tee 23, 12618 Tallinn, Estonia*

[2]*Department of Physics, Budapest University of Technology and Economics and MTA-BME Lendület Magneto-optical Spectroscopy Research Group, 1111 Budapest, Hungary*

[3]*Condensed Matter Research Group of the Hungarian Academy of Sciences, 1111 Budapest, Hungary*

[4]*Institute of Solid State Physics, Vienna University of Technology, 1040 Vienna, Austria*

[5]*RIKEN Center for Emergent Matter Science (CEMS), Wako 351-0198, Japan*

[6]*Hungarian Academy of Sciences, Premium Postdoctor Program, 1051 Budapest, Hungary*

[7]*Experimental Physics V, Center for Electronic Correlations and Magnetism, Institute of Physics, University of Augsburg, 86159 Augsburg, Germany*

[8]*High Field Magnet Laboratory (HFML-EMFL), Radboud University, Toernooiveld 7, 6525 ED Nijmegen, Netherlands*

[9]*National High Magnetic Field Laboratory, Tallahassee, FloridA 32310, USA*

[10]*Department of Physics, Florida A&M University, Florida 32307, USA*

[11]*National Institute of Advanced Industrial Science and Technology (AIST), Tsukuba, 305-8565 Ibaraki, Japan*

[12]*Department of Chemistry and Physics, Augusta University, 1120 15th Street, Augusta, Georgia 30912, USA*

[13]*Materials Science and Technology Division, Oak Ridge National Laboratory, Oak Ridge, Tennessee 37830, USA*

(Received 26 September 2020; accepted 18 November 2020; published 9 December 2020)

Using THz spectroscopy, we show that the spin-wave spectrum of multiferroic $BiFeO_3$ in its high-field canted antiferromagnetic state is well described by a spin model that violates rhombohedral symmetry. We demonstrate that the monoclinic distortion of the canted antiferromagnetic state is induced by the single-ion magnetoelastic coupling between the lattice and the two nearly antiparallel spins. The revised spin model for $BiFeO_3$ contains two new single-ion anisotropy terms that violate rhombohedral symmetry and depend on the direction of the magnetic field.

DOI: 10.1103/PhysRevB.102.214410

I. INTRODUCTION

Room-temperature multiferroic $BiFeO_3$ is one of the most technologically important materials in the rapidly expanding field of spintronics [1–3], with applications to nanoelectronics [4,5] and photo-voltaics [6,7]. One of the most useful ways to control the properties of $BiFeO_3$ thin films is through strain, which unwinds the cycloidal spin state and stabilizes a canted G-type antiferromagnet (AF) [8,9]. Increasing epitaxial strain transforms the structure of thin films from rhombohedral to tetragonal-like monoclinic [10–12]. Recent work on thin films [13,14] reveals that epitaxial strain can rotate the AF vector $\mathbf{S}_1 - \mathbf{S}_2$ with respect to the electric polarization $\mathbf{P}$. Despite great interest in controlling its magnetic properties, comparatively little is known about the effects of magnetoelastic strain on bulk $BiFeO_3$ [15].

Magnetic properties of bulk materials are typically described by spin Hamiltonians with constant parameters. Due to magnetostriction, however, those parameters may depend on field and temperature. In ferromagnetic (FM) materials, a large magnetic moment strains the crystal and the strain changes the spin couplings [16–19]. Less is known about the effects of magnetostriction on AF materials or on materials with weak FM moments, where the most notable manifestation of magnetostriction appears to be a spontaneous or field-induced spin reorientation [18,20,21].

A small, canted magnetic moment less than 0.1 μ_B appears just above 18 T in the G-type AF phase of $BiFeO_3$ [22–25]. The spin model of $BiFeO_3$ in this canted phase is not well understood because high fields present challenges for both structural and spectroscopic probes. In this paper, we describe the THz absorption by spin waves in the high-field canted phase of $BiFeO_3$. Based on high-resolution measurements of the spin-wave frequencies, we show that the change of symmetry from rhombohedral to monoclinic activates two new coupling terms in the spin Hamiltonian. This paper demonstrates that THz measurements can be used to determine the magnetoelastic coupling constants in the AF phase of $BiFeO_3$.

Following the appearance of the electric polarization $\mathbf{P}$ along one of the pseudocubic diagonals, the cubic symmetry of the perovskite structure of bulk $BiFeO_3$ is broken below $T_c \approx 1100$ K [26–28]. A cycloidal spin state with wave vector $\mathbf{Q} \perp \mathbf{P}$ and spins predominantly in the plane defined by $\mathbf{Q}$ and $\mathbf{P}$ develops below $T_N \approx 640$ K [29–31]. In zero magnetic

*toomas.room@kbfi.ee
†fishmanrs@ornl.gov

field, the cycloid has a wavelength of 62 nm [29,32–34]. An applied magnetic field increases the wavelength and rotates **Q** [35]. When a field applied perpendicular to **P** exceeds $B_c \approx 18$ T, the cycloid transforms into a G-type AF [36]. Both the polarization **P** and the magnetization **M** exhibit steplike changes at B_c [22,37].

Although the crystal structure of bulk ferroelectric $BiFeO_3$ was first assigned to the rhombohedral space group $R3c$ [28,38–41], high-resolution structural studies suggested that the crystal symmetry might be monoclinic Cc [42] or even lower, triclinic $P1$ [43]. Additional evidence for broken symmetry comes from magnetostriction measurements: As the cycloid unwinds in a magnetic field, the contraction or expansion of the lattice depends on the direction of the applied field [15]. Based on a study of the THz absorption spectra in the high-field canted AF phase, this paper shows that magnetoelastic coupling transforms the crystal structure of $BiFeO_3$ from rhobomhedral to monoclinic. A new microscopic model for the canted AF phase contains two new single-ion anisotropy terms that break rhombohedral symmetry and depend on the orientation of the magnetic field.

Many years and tremendous effort have been spent constructing the spin model for bulk $BiFeO_3$. Much has been learned about the microscopic parameters by studying the spin-wave excitations of the cyloidal state using four different methods: inelastic neutron scattering (INS) [44–47], Raman [48,49], submillimeter wave electron spin resonance (ESR) [50], and THz [51–54] spectroscopies. Because few sub-THz spectroscopic methods are compatible with high magnetic fields [50,52], much less is known about the spin-wave excitations in the canted AF state.

The two iron $S = 5/2$ spins in the G-type AF structure produce two spin-wave modes, ν_1 and ν_2. In earlier measurements, crystals were grown by the flux method, which provided platelets with a large surface parallel to (001) crystal plane (pseudocubic notation). The lower frequency mode ν_1 was then observed by ESR [50] and the upper mode ν_2 by THz absorption spectroscopy [52] with field along (001). The dependence of the mode frequencies on the field direction was not studied.

In the present paper, a large single crystal grown using the floating zone method [55] was cut into 0.5-mm-thick samples with large faces normal to [1,−1,0], [−1, −1,2] and [1,1,1]. THz absorption measurements employed either Fourier transform far-infrared (FIR) or continuous wave (CW) spectroscopy. FIR measurements were performed above 0.55 THz in a fixed magnetic field. CW measurements were performed at a fixed frequency between 0.1 and 0.9 THz by sweeping the magnetic field, a method also called submillimeter wave ESR. Radiation propagated either parallel (Faraday configuration) or perpendicular (Voigt configuration) to the applied magnetic field. Descriptions of the experiment and measured spectra are provided in the Supplemental Material [56].

In low fields and temperatures, it is sufficient to treat the exchange, Dzyaloshinskii-Moriya (DM), and single-ion anisotropy parameters as constants. At high magnetic fields, however, magnetoelastic coupling (magnetostriction) distorts the lattice and can change those parameters. In a FM, Callen and Callen [16–19] showed that the driving force of magnetoelastic coupling is the macroscopic magnetic moment, which changes with temperature or in a magnetic field. However, AFs do not have a net magnetic moment. In $BiFeO_3$, the DM interaction and magnetic field cant the spins but the net magnetic moment is very weak.

To study the magnetoelastic properties of an AF, we expand the free energy in terms of the strain and the FM and AF ordering vectors, $\mathbf{S}_1 + \mathbf{S}_2$ and $\mathbf{S}_1 - \mathbf{S}_2$ [20]. But calculating the spin-wave spectrum using this approach requires an exact spin-operator form for the magnetoelastic coupling. This paper shows that THz spectroscopy can be used to narrow down the possible magnetoelastic coupling terms in the Hamiltonian and to determine the small coupling parameters.

This paper is divided into five sections. Section II describes the new spin model for $BiFeO_3$ in the high-field canted phase. Predictions of that model are compared with THz measurements in Sec. III and the resulting model parameters are presented in Sec. IV. Section V contains a discussion and conclusion. In the Supplemental Material [56], we derive the possible magnetoelastic coupling terms consistent with monoclinic symmetry for $BiFeO_3$.

II. MODEL

This section develops a new spin model for $BiFeO_3$ by applying the microscopic theory of Callen *et al.* [16,18] to the canted AF state. Even in the absence of a net magnetic moment, strain couples to the nearly collinear spins $\mathbf{S}_1$ and $\mathbf{S}_2$ in the magnetic unit cell. Due to crystal fields, this magnetoelastic coupling affects the local single-ion anisotropy parameters of the spin Hamiltonian. Details of this treatment are provided in the Supplemental Material [56].

The earlier rhombohedral spin model of the cycloidal spin state contained two exchange constants, two DM terms, and one anisotropy term:

$$\begin{aligned}\mathcal{H}_{\rm m} = &-J_1 \sum_{\langle i,j\rangle} \mathbf{S}_i \cdot \mathbf{S}_j - J_2 \sum_{\langle i,j\rangle'} \mathbf{S}_i \cdot \mathbf{S}_j \\ &+ D_1 \sum_{\langle i,j\rangle} (\mathbf{Z} \times \mathbf{e}_{i,j}/a) \cdot (\mathbf{S}_i \times \mathbf{S}_j) \\ &+ D_2 \sum_{\langle i,j\rangle} (-1)^{h_i} \mathbf{Z} \cdot (\mathbf{S}_i \times \mathbf{S}_j) - K_Z \sum_i S_{iZ}^2 \\ &- \frac{1}{2} K_H \sum_i [(S_{iX} + iS_{iY})^6 + (S_{iX} - iS_{iY})^6] \\ &- g\mu_{\rm B} B \sum_i \mathbf{m} \cdot \mathbf{S}_i, \end{aligned} \tag{1}$$

where $\mathbf{e}_{i,j} = a\mathbf{x}$, $a\mathbf{y}$, or $a\mathbf{z}$ connects the $S = 5/2$ spin $\mathbf{S}_i$ on site $\mathbf{R}_i$ with the nearest-neighbor spin $\mathbf{S}_j$ on site $\mathbf{R}_j = \mathbf{R}_i + \mathbf{e}_{i,j}$. The integer $h_i = \sqrt{3}\mathbf{R}_i \cdot \mathbf{Z}/a$ is the hexagonal layer number. While the AF exchange J_1 couples nearest-neighbor spins along the edges of the cube, the AF exchange J_2 couples next-nearest-neighbor spins along the cube face diagonals, Fig. 1. Easy-axis anisotropy K_Z lies along the polarization direction **Z**. Hexagonal anisotropy [57,58] K_H pins the plane of the cycloid and the cycloidal wave vector **Q** to one of the hexagonal axis $[1, -1, 0]$, $[0, 1, -1]$ or $[1, 0, -1]$ perpendicular to **Z**. The last term in Eq. (1) is the interaction of spin $\mathbf{S}_i$ with

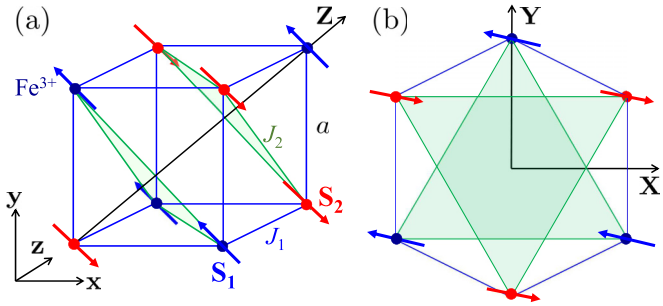

FIG. 1. (a) The crystallographic pseudocubic unit cell of $BiFeO_3$. In the canted AF state, the magnetic unit cell is $2a \times 2a \times 2a$ with two spins, $\mathbf{S}_1$ and $\mathbf{S}_2$, per unit cell and pseudocubic unit vectors $\mathbf{x} = [1, 0, 0]$, $\mathbf{y} = [0, 1, 0]$, and $\mathbf{z} = [0, 0, 1]$. (b) Fragments of two nearest-neighbor hexagonal planes viewed along $\mathbf{Z}$. In the hexagonal planes (shaded triangles) normal to $\mathbf{Z} = [1, 1, 1]/\sqrt{3}$, the unit vectors are $\mathbf{X} = [1, -1, 0]/\sqrt{2}$ and $\mathbf{Y} = [-1, -1, 2]/\sqrt{6}$.

a magnetic field $\mathbf{B} = B\mathbf{m}$. We assume that the g factor for the $S = 5/2$ iron spins is isotropic with $g = 2$.

Two DM interactions are produced by broken inversion symmetry. While the first DM interaction D_1 determines the cycloidal period λ [59], the second DM interaction D_2 tilts the cycloid out of the plane defined by $\mathbf{Z}$ and the ordering wave vector $\mathbf{Q} \perp \mathbf{Z}$ [22,59,60]. Because this tilt averages to zero over the length of the cycloid, $BiFeO_3$ has no spontaneous magnetic moment below B_c. In the canted AF state above B_c, $BiFeO_3$ has a small ferrimagnetic moment perpendicular to $\mathbf{P}$ [22–25].

Exchange parameters J_1 and J_2 are taken from INS [44–46], which measured the spin-wave spectra over a wide range of energies and wave vectors. Because INS lacks sufficient wave vector resolution, the smaller DM and anisotropy terms were later estimated using THz absorption spectroscopy [52]. For convenience, Table I summarizes the values of these parameters and the experimental or theoretical methods used for their determination based on the properties of the cycloidal state assuming rhombohedral $R3c$ symmetry.

The spin model for $BiFeO_3$ undergoes significant simplifications in the high-field canted AF state. Due to the steep dispersion $\omega = cq$ of photons, THz spectroscopy measures the spin-wave frequencies at wave vector $q \ll 2\pi/a$. With two spins in the cubic unit cell shown in Fig. 1, J_2 does not contribute when $\mathbf{q} \approx 0$ [61]. It is also easy to show that the first DM interaction D_1 has no effect on the mode frequencies in the canted AF state because it sums to zero. Taking $J_1 \approx -5.3$ meV from INS measurements [44–46], $\mathcal{H}_{\rm m}^{\rm AF}$ only depends on the DM interaction parameter D_2 and the anisotropy parameters K_Z and K_H:

$$\mathcal{H}_{\rm m}^{\rm AF} = -J_1 \sum_{\langle i,j \rangle} \mathbf{S}_i \cdot \mathbf{S}_j + D_2 \sum_{\langle i,j \rangle} (-1)^{h_i}\, \mathbf{Z} \cdot (\mathbf{S}_i \times \mathbf{S}_j) - K_Z \sum_i S_{iZ}^2 - \frac{1}{2} K_H \sum_i [(S_{iX} + iS_{iY})^6 + (S_{iX} - iS_{iY})^6]$$

TABLE I. Exchange and anisotropy parameters, unit meV, of $BiFeO_3$. The spin-wave energies at $\mathbf{q} = 0$ do not depend on the parameters J_2 and D_1 in the canted AF state. K_H is hexagonal anisotropy [57,58] used to model the rhombohedral phase (see Supplemental Material). Magnetoelastic anisotropy parameters $K_{E,2}$ and $K_{E,3}$ were determined for the magnetic-field directions $\mathbf{X}$, $\mathbf{Y}$, and $\mathbf{z}$. By symmetry, magnetoelastic anisotropy parameters are zero when $\mathbf{B} \parallel \mathbf{Z}$.

	Previous	Method	This paper
J_1	-5.3	[a]	-5.3 (fixed)
J_2	-0.2	[a]	-
D_1	0.18	[b]	-
D_2	6.0×10^{-2}	[c]	$(8.32 \pm 0.48) \times 10^{-2}$
K_Z	4.0×10^{-3}	[d]	$(3.76 \pm 0.39) \times 10^{-3}$
K_H	4×10^{-6}	[e]	0
	Magnetic field direction (this paper)		
	X		**Y**, **z**
$K_{E,2}$	0		$(1.02 \pm 0.27) \times 10^{-4}$
$K_{E,3}$	$-(5.90 \pm 0.68) \times 10^{-5}$		$-(1.14 \pm 0.61) \times 10^{-5}$

[a]INS [44–46]
[b]Cycloid wavelength [59]
[c]Cycloid tilt [23,64], INS [47]
[d]Third harmonic generation [65,66], neutron diffraction [36], INS [45,47], spectroscopy [52,67], tight binding [68]
[e]Cycloid order vector rotation [57,58]

$$- g\mu_{\rm B} B \sum_i \mathbf{m} \cdot \mathbf{S}_i. \tag{2}$$

Hexagonal anisotropy is the weakest interaction in this Hamiltonian with $K_H S^6 < 10^{-3}$ meV. Since $|D_2| \gg K_Z$, the spins lie primarily in the XY plane with $\langle S_{iZ} \rangle \approx 0$. The spin canting induced by the DM interaction and by magnetic fields [15] up to about 35 T is less than 2°. Consequently, the zero-order spin state is $\mathbf{S}_1 \approx -\mathbf{S}_2$ and $(\mathbf{S}_1 - \mathbf{S}_2) \perp \mathbf{B}$.

Because the spins are perpendicular to the field $\mathbf{B}$, the magnetoelastic strain depends on the field direction $\mathbf{m}$. The equilibrium strain is solved by minimizing the elastic and magnetoelastic energies for field directions $\mathbf{X}$ and $\mathbf{Y}$, see Supplemental Material [56]. When $\mathbf{B} \parallel \mathbf{Z}$, there is no preferred orientation for the spins in the hexagonal plane and the strain vanishes. For $\mathbf{B} \parallel \mathbf{X}$, the zero-order spin state has $(\mathbf{S}_1 - \mathbf{S}_2) \parallel \mathbf{Y}$. For $\mathbf{B} \parallel \mathbf{z}$ or $\parallel \mathbf{Y}$, the zero-order spin state has $(\mathbf{S}_1 - \mathbf{S}_2) \parallel \mathbf{X}$ because both $\mathbf{z}$ and $\mathbf{Y}$ are perpendicular to $\mathbf{X} = (\mathbf{x} - \mathbf{y})/\sqrt{2}$.

Both the strain and the unit vectors $\mathbf{X}_n$ and $\mathbf{Y}_n$ are determined by the field direction $\mathbf{m}$. Hence, our analysis would be the same for $\mathbf{B}$ along any cubic axis. If $\mathbf{B} \parallel \mathbf{x}$, then the spins $\mathbf{S}_1$ and $\mathbf{S}_2$ would point (approximately) along $\pm\mathbf{X}_3$ with $\mathbf{X}_3 \equiv [0, 1, -1]/\sqrt{2} \perp \mathbf{x}$. If $\mathbf{B} \parallel \mathbf{y}$, then the spins would point along $\pm\mathbf{X}_2$ with $\mathbf{X}_2 \equiv [-1, 0, 1]/\sqrt{2} \perp \mathbf{y}$. For specificity, we treat the case $\mathbf{B} \parallel \mathbf{z}$ with $\mathbf{X} = \mathbf{X}_1 \equiv [1, -1, 0]/\sqrt{2} \perp \mathbf{z}$. In all cases, $\mathbf{Y}_n = \mathbf{Z} \times \mathbf{X}_n$.

The new spin state and spin-wave frequencies are modeled by the Hamiltonian

$$\mathcal{H} = \mathcal{H}_{\rm m}^{\rm AF} + \sum_i \mathcal{H}_{\rm me}^i(\mathbf{m}), \tag{3}$$

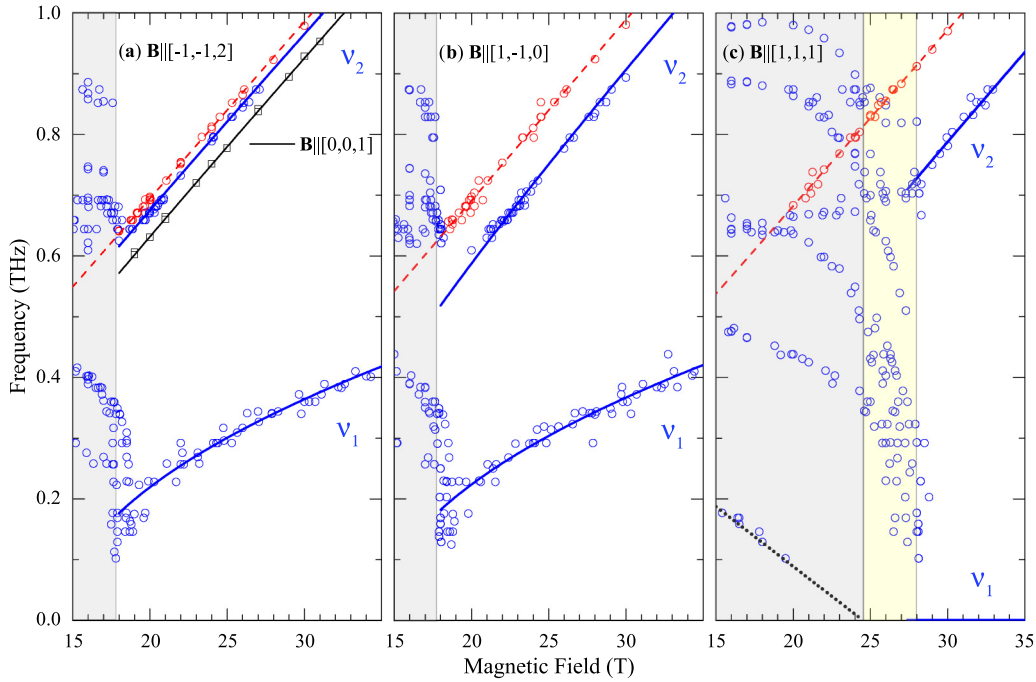

FIG. 2. Spin-wave frequencies at liquid He temperature for field along (a) **Y** (blue circles and blue lines) and **z** (black squares and black line, data from [52]), (b) **X**, or (c) **Z**. Experimental points are marked by blue circles and black squares. Solid lines are the best fits for spin-wave modes ν_1 and ν_2 using Eq. (3). The dashed red line is the linear fit of impurity peak positions, red circles. The black dotted line in panel (c) is the linear extrapolation of the frequency dependence of mode $\Phi_1^{(1)}$ in the cycloidal state [54]. The gray background denotes the cycloidal state. The yellow background denotes the intermediate spin state between the cycloidal and canted AF states for $\mathbf{B} \parallel \mathbf{Z}$ in panel (c). The boundaries are determined from the field dependence of the magnetization $M(B)$ [63].

where the new strain-induced Hamiltonian for the ith spin is

$$\begin{aligned}\mathcal{H}^i_{\rm me}(\mathbf{m}) = &-K^{(\mathbf{m})}_{A,1} S_{iY} S_{iZ} - K^{(\mathbf{m})}_{A,2}\left(S^2_{iX} - S^2_{iY}\right)\\ &- K^{(\mathbf{m})}_{E,1} S_{iY} S^3_{iZ} - K^{(\mathbf{m})}_{E,2}\left(S^2_{iX} - S^2_{iY}\right) S^2_{iZ}\\ &- K^{(\mathbf{m})}_{E,3}\left(S^4_{iX} + S^4_{iY} - 6 S^2_{iX} S^2_{iY}\right) \qquad (4)\end{aligned}$$

and the single-ion anisotropy constants depend on the field orientation **m**. As shown in the Supplemental Material, the two strains $\epsilon_1^{\gamma,1} = \frac{1}{2}[\epsilon_{XX} - \epsilon_{YY}]$ and $\epsilon_1^{\gamma,2} = \epsilon_{YZ}$ couple to the zero-order spin state [56].

III. COMPARISON WITH THZ MEASUREMENTS

For each field direction and magnitude, the energy $E = \langle \mathcal{H} \rangle$ was minimized as a function of angles θ_i and ϕ_i for the two spins $\mathbf{S}_i = S(\cos\phi_i \sin\theta_i \mathbf{X} + \sin\phi_i \sin\theta_i \mathbf{Y} + \cos\theta_i \mathbf{Z})$ in the unit cell. Linear spin-wave theory was then used to evaluate the two spin-wave mode frequencies, which were compared with the measured frequencies. This loop was repeated by varying the Hamiltonian parameters until a minimum χ^2 was achieved [62].

Measured mode frequencies are plotted as a function of magnetic field along **X**, **Y**, **Z**, and cubic axis **z** in Fig. 2. The blue circles and black squares are the spin-wave frequencies. The red dashed line gives the linear field dependence of the red circles, which are produced by impurities [56].

The boundaries between the cycloidal and canted AF state found by THz absorption spectroscopy agree fairly well with the vertical lines in Fig. 2 obtained from the the maximum of $\mathrm{d}M/\mathrm{d}B$, where $M(B)$ is the magnetization [25,63]. For the field along **Z**, $\mathrm{d}^2M/\mathrm{d}B^2$ vanishes at the upper critical field of the intermediate state, 28 T. Scattering of the THz data near 18 T for field along **X** or **Y**, Figs. 2(a) and 2(b), is probably caused by a slight misorientation of the sample relative to $\mathbf{B} \parallel \mathbf{Z}$.

At 28 T, the transition into the canted AF state for $\mathbf{B} \parallel \mathbf{Z}$ is clearly marked by the appearance of the ν_2 mode and the disappearance of other modes, Fig. 2(c). Since strain is absent and there is no in-plane anisotropy for this field direction (we assume $K_H = 0$), our model predicts that $\nu_1 = 0$.

An intermediate spin state appears between the cycloidal and canted AF states when $\mathbf{B} \parallel \mathbf{Z}$, Fig. 2(c). In the cycloidal state, the frequency of mode $\Phi_1^{(1)}$ [[54]] extrapolates to zero at 24.5 T, the same field where the cycloidal state transforms to an intermediate state according to magnetization data. Other modes do not exhibit clear changes when entering this intermediate state. Theoretical studies [69] and neutron diffraction spectroscopy [15,70] reveal that the intermediate state in magnetic field $\mathbf{B} \parallel \mathbf{Z}$ is a conical spin structure with ordering vector along the magnetic field. While earlier measurements suggested that it disappears at low T [15], our data indicate that the intermediate state exists even at low T when $\mathbf{B} \parallel \mathbf{Z}$.

Our main theoretical results for the spin-wave frequencies are shown by the solid curves in Fig. 2, which were obtained for a magnetoelastically strained crystal using Eq. (3). We introduce ten strain-induced parameters $K^{(\mathbf{m})}_{\Gamma,k}$: one set for $\mathbf{m} = \mathbf{X}$ and the other set for $\mathbf{m} = \mathbf{Y}$ or **z**. Recall that strain is absent for $\mathbf{m} \parallel \mathbf{Z}$. Because the spins lie in the XY plane, $-K^{(\mathbf{m})}_{E,1} \sum_i S_{iY} S^3_{iZ}$ does not contribute to the spin dynamics

(only two of the three factors of S_{iZ} can be replaced by boson operators in the Holstein-Primakoff expansion [62]). Our fit gave large errors for the parameters $K_{A,1}^{(\mathbf{m})}$, $K_{A,2}^{(\mathbf{m})}$, and $K_{E,2}^{(\mathbf{m}=\mathbf{X})}$, which were then set to zero. Consequently, neither of the $l = 2$ monoclinic, single-ion anisotropy terms appear in our Hamiltonian. Found to be negligible, K_H was also set to zero. The final fit was then performed with three magnetostriction-enforced parameters together with D_2 and K_Z: five parameters in all [71]. Table I lists the values for these five parameters.

Aside from some differences due to the scattering of the experimental points (particularly for ν_1), the agreement between theory and experiment for the THz frequencies is quite good. By contrast, the rhombohedral spin model yields a value for χ^2 that is four times larger [56] than our monoclinic model.

IV. MODEL PARAMETERS

Table I compares the parameters of the canted AF and cycloidal states. While the new estimate for K_Z is close to the previous estimate in the cycloidal state, the new value for D_2 is about 39% larger than the cycloidal estimate.

Our numerical results for the anisotropy parameters agree with simple estimates based on their order in the spin-orbit coupling parameter $l|J_1|$ where $l \sim 10^{-1}$. While the DM interactions are first order in l and the easy-axis anisotropy K_Z is second order in l, the magnetoelastic parameters $K_{E,2}$ and $K_{E,3}$ are third order [57]. Therefore, $S^4 K_{E,n} \sim lS^2 K_Z$ so $K_{E,n} \sim 10^{-2} K_Z$, as found in Table I. Just as INS lacks the energy resolution to determine the small DM and anisotropy interactions in $BiFeO_3$, it also lacks the energy resolution to determine the even smaller magnetoelastic coupling parameters $K_{E,2}$ and $K_{E,3}$. Fortunately, the small parameters induced by spin-orbit coupling can be measured using spectroscopic techniques.

As expected, the canted AF state has a small FM moment in the XY plane induced by the DM interaction D_2. The spin canting and corresponding FM moment M_0 can be experimentally estimated by extrapolating the magnetization to zero magnetic field. While early work [72] estimated that $M_0 = 0.03\ \mu_B$ per Fe, more recent experiments obtained $M_0 = 0.048\ \mu_B$ [73] or $0.04\ \mu_B$ [15] per Fe.

With spins in the XY plane and $K_H = 0$, only the $K_{E,3}^{(\mathbf{m})}$ term violates rotational invariance. The canting angle $\phi_0 \ll 1$ is theoretically given by

$$\phi_0 \approx \frac{1}{2}\frac{D_2}{|J_1| + K_{E,3}^{(\mathbf{m})} S^2/3}, \tag{5}$$

with canted magnetization:

$$M_0 = 2S\mu_B \sin\phi_0 \approx \frac{S\mu_B D_2}{|J_1| + K_{E,3}^{(\mathbf{m})} S^2/3}. \tag{6}$$

Because $K_{E,3}^{(\mathbf{m})} S^2/3|J_1| \sim 10^{-5}$, $\phi_0 \approx D_2/2|J_1|$, and $M_0 \approx S\mu_B D_2/|J_1|$ are independent of the direction of the field in the XY plane, in agreement with the observation that M_0 is the same for fields along $\mathbf{X}$ and $\mathbf{Y}$ [73]. The rotational invariance of M_0 confirms that magnetostriction affects neither the exchange coupling J_1 nor the DM coupling D_2: if J_1 or D_2 were altered by strain, then $M_0 \propto D_2/|J_1|$ would be different for fields along $\mathbf{X}$ and $\mathbf{Y}$. Our result that magnetostriction mostly affects the single-ion anisotropy is consistent with recent *ab initio* results that the single-ion anisotropy is highly sensitive to a small misfit of crystal parameters [14].

The fitting parameter $D_2 \approx 8.3 \times 10^{-2}$ meV gives $\phi_0 = 0.0078 \pm 0.0005$ rad and $M_0 \approx 0.039 \pm 0.002\ \mu_B$ per Fe, which is within range of the two most recent experimental estimates [15,73]. By comparison, the value $D_2 \approx 6.0 \times 10^{-2}$ meV obtained from earlier cycloidal state measurements [23,47,64] and from a rhombohedral fit for the canted AF state [56] gives $M_0 = 0.027\ \mu_B$ per Fe, which is about 33% smaller than the recent experimental estimate of $0.04\ \mu_B$ [15].

V. DISCUSSION AND CONCLUSION

Since $K_{E,2}^{(\mathbf{m})}$ and $K_{E,3}^{(\mathbf{m})}$ depend on the direction $\mathbf{m}$ of the magnetic field, the strain is different for fields along $\mathbf{X}$ and $\mathbf{Y}$. This agrees with the observation that the magnetostriction $\Delta l_X/l_X$ at $\mathbf{B}_c$ [74] is positive when $\mathbf{B} \parallel \mathbf{X}$ and negative when $\mathbf{B} \parallel \mathbf{Y}$. Moreover, $\Delta l_X/l_X$ is nearly constant as B increases above the critical field. Hence, the single-ion contributions of the spin-canting FM component $\mathbf{S}_1 + \mathbf{S}_2$ to the magnetostriction are small compared to the single-ion contributions of the AF vector $\mathbf{S}_1 - \mathbf{S}_2$.

Other evidence for magnetoelastic coupling in the canted AF state is provided by the transverse electric polarization $\mathbf{P}_t \perp \mathbf{Z}$, which changes as the magnetic field is rotated in the hexagonal plane [74]. If $\mathbf{m} \parallel \mathbf{Y}$, $\mathbf{P}_t \parallel \mathbf{Y}$; if $\mathbf{m} \parallel \mathbf{X}$, $\mathbf{P}_t \parallel -\mathbf{Y}$. Both strains $\epsilon_1^{\gamma,1} = [\epsilon_{XX} - \epsilon_{YY}]/2$ and $\epsilon_1^{\gamma,2} = \epsilon_{YZ}$ preserve the YZ mirror plane and allow $\mathbf{P}_t \parallel \mathbf{Y}$. Because ϵ_{YZ} tilts the Z axis, it could produce the in-plane component $\mathbf{P}_t$ by rotating the FE polarization $\mathbf{P}$. A tilting angle of 0.01 to 0.04° is consistent with the magnitude of P_t [15].

In the cycloidal state, $\mathbf{P}_t$ is again modulated by the rotation of an in-plane magnetic field with an amplitude roughly half the size of that in the AF state [74]. Unlike in the canted AF state, this behavior cannot be explained by the strain ϵ_{YZ} because a periodic spin structure like the cycloid should not produce homogeneous strain. Therefore, it is likely [74] that $\mathbf{P}_t$ is induced by metal-ligand hybridization [75] and not by the tilting of the c axis in both the cycloidal and AF states. Additional magnetostriction measurements are needed to determine which strain component, $\epsilon_1^{\gamma,1} = [\epsilon_{XX} - \epsilon_{YY}]/2$ or $\epsilon_1^{\gamma,2} = \epsilon_{YZ}$, is dominant in the AF state of $BiFeO_3$.

The hysteresis of the magnetostriction [15] and of the cycloidal wave vector $\mathbf{Q}$ in a magnetic field [35] also demonstrate that magnetoelastic coupling is important in the cycloidal state. The rotation of the AF vector $\mathbf{S}_1 - \mathbf{S}_2$ with the period of the cycloidal wavelength will induce strain at the harmonic wave vectors $2Q$ and $4Q$. Consequently, the single-ion anisotropy constants will also be modulated with wave vectors $2Q$ and $4Q$. However, the spin-wave frequencies of the cycloidal state are (at least so far) well described by the rhombohedral model without additional magnetoelastic couplings.

This paper demonstrates that high-resolution THz absorption measurements can be used to determine the magnetoelastic coupling constants for the AF phase of a material. The magnetic-field dependence of the $\mathbf{q} = 0$ spin-wave frequencies in the canted AF state of $BiFeO_3$ were fitted using a

spin model consistent with the monoclinic distortion of the orthorhombic $R3c$ lattice. Whereas epitaxial strain stabilizes the monoclinic phase in thin $BiFeO_3$ films [10], magnetoelastic coupling stabilizes the monoclinic phase in bulk $BiFeO_3$. The magnetoelastic coupling is driven by the in-plane spin components parallel to the AF order vector $\mathbf{S}_1 - \mathbf{S}_2$. Those spin components couple to the strain through single-ion anisotropy interactions. Our new microscopic model for the canted AF state of $BiFeO_3$ contains two single-ion terms that only appear in monoclinic symmetry and depend on the direction of the magnetic field in the XY plane. The dependence of the spin microscopic parameters on the orientation of the magnetic field has clear implications for the technological applications of $BiFeO_3$.

Several new questions about bulk $BiFeO_3$ are raised by this work. Density-functional calculations are needed to understand the disappearance of the $l = 2$ single-ion anisotropy terms. Magnetostriction measurements are required to distinguish the strains $\epsilon_1^{\gamma,1} = [\epsilon_{XX} - \epsilon_{YY}]/2$ and $\epsilon_1^{\gamma,2} = \epsilon_{YZ}$ in the canted AF state. The appearance of the intermediate conical state for the field along $\mathbf{Z}$ at low temperatures requires additional study. New measurements and theory are needed to clarify the role of magnetoelastic coupling in the cycloidal state. Thus, the proposed model may serve as the foundation for future work on this important multiferroic material, providing insight into both the cycloidal and canted AF states.

ACKNOWLEDGMENTS

We thank Bianca Trociewitz for her contribution to the design of probes and for technical assistance in Tallahassee. Research was supported by the European Regional Development Fund Project No. TK134 and by the Estonian Ministry of Education and Research Council Grants No. IUT23-03 and No. PRG736, by the bilateral program of the Estonian and Hungarian Academies of Sciences under Contract No. SNK-64/2013, by the Hungarian NKFIH Grants No. K 124176 and No. ANN 122879, by the BME-Nanonotechnology and Materials Science FIKP grant of EMMI (BME FIKP-NAT), by the FWF Austrian Science Fund I 2816-N27, and by the Deutsche Forschungsgemeinschaft (DFG) via the Transregional Research Collaboration TRR 80: From Electronic Correlations to Functionality (Augsburg-Munich-Stuttgart). T.D. acknowledges funding support from Augusta University and SYSU Grant No. OEMT-2017-KF-06 and R.S.F. by the U.S. Department of Energy, Office of Basic Energy Sciences, Materials Sciences and Engineering Division. A portion of this work was performed at the National High Magnetic Field Laboratory, which is supported by NSF Cooperative Agreement No. DMR-1644779 and the State of Florida. The support of the HFML-RU/FOM, member of the European Magnetic Field Laboratory (EMFL), is acknowledged.

This paper has been authored by UT-Battelle, LLC under Contract No. DE-AC05-00OR22725 with the U.S. Department of Energy. The U.S. Government retains and the publisher, by accepting the article for publication, acknowledges that the U.S. Government retains a nonexclusive, paid-up, irrevocable, worldwide license to publish or reproduce the published form of this paper, or allow others to do so, for U.S. Government purposes. The Department of Energy will provide public access to these results of federally sponsored research in accordance with the DOE Public Access Plan [76].

[1] S. Manipatruni, D. E. Nikonov, and I. A. Young, Beyond CMOS computing with spin and polarization, Nat. Phys. **14**, 338 (2018).

[2] S. Manipatruni, D. E. Nikonov, C.-C. Lin, T. A. Gosavi, H. Liu, B. Prasad, Y.-L. Huang, E. Bonturim, R. Ramesh, and I. A. Young, Scalable energy-efficient magnetoelectric spin-orbit logic, Nature **565**, 35 (2019).

[3] N. A. Spaldin and R. Ramesh, Advances in magnetoelectric multiferroics, Nat. Mater. **18**, 203 (2019).

[4] A. Crassous, R. Bernard, S. Fusil, K. Bouzehouane, D. Le Bourdais, S. Enouz-Vedrenne, J. Briatico, M. Bibes, A. Barthélémy, and J. E. Villegas, Nanoscale Electrostatic Manipulation of Magnetic Flux Quanta in Ferroelectric/Superconductor $BiFeO_3/YBa_2$ Cu_3 $O_{7-\delta}$ Heterostructures, Phys. Rev. Lett. **107**, 247002 (2011).

[5] J.-C. Yang, Q. He, P. Yu, and Y.-H. Chu, $BiFeO_3$ thin films: A playground for exploring electric-field control of multifunctionalities, Annu. Rev. Mater. Res. **45**, 249 (2015).

[6] S. Y. Yang, L. W. Martin, S. J. Byrnes, T. E. Conry, S. R. Basu, D. Paran, L. Reichertz, J. Ihlefeld, C. Adamo, A. Melville, Y.-H. Chu, C.-H. Yang, J. L. Musfeldt, D. G. Schlom, J. W. Ager, and R. Ramesh, Photovoltaic effects in $BiFeO_3$, Appl. Phys. Lett. **95**, 062909 (2009).

[7] E. Parsonnet, Y.-L. Huang, T. Gosavi, A. Qualls, D. Nikonov, C.-C. Lin, I. Young, J. Bokor, L. W. Martin, and R. Ramesh, Toward Intrinsic Ferroelectric Switching in Multiferroic $BiFeO_3$, Phys. Rev. Lett. **125**, 067601 (2020).

[8] F. Bai, J. Wang, M. Wuttig, JieFang Li, N. Wang, A. P. Pyatakov, A. K. Zvezdin, L. E. Cross, and D. Viehland, Destruction of spin cycloid in $(111)_c$-oriented $BiFeO_3$ thin films by epitiaxial constraint: Enhanced polarization and release of latent magnetization, Appl. Phys. Lett. **86**, 032511 (2005).

[9] C. Ederer and N. A. Spaldin, Weak ferromagnetism and magnetoelectric coupling in bismuth ferrite, Phys. Rev. B **71**, 060401(R) (2005).

[10] H. Béa, M. Bibes, S. Petit, J. Kreisel, and A. Barthélémy, Structural distortion and magnetism of $BiFeO_3$ epitaxial thin films: A Raman spectroscopy and neutron diffraction study, Philos. Mag. Lett. **87**, 165 (2007).

[11] M. N. Iliev, M. V. Abrashev, D. Mazumdar, V. Shelke, and A. Gupta, Polarized Raman spectroscopy of nearly tetragonal $BiFeO_3$ thin films, Phys. Rev. B **82**, 014107 (2010).

[12] G. J. MacDougall, H. M. Christen, W. Siemons, M. D. Biegalski, J. L. Zarestky, S. Liang, E. Dagotto, and S. E. Nagler, Antiferromagnetic transitions in tetragonal-like $BiFeO_3$, Phys. Rev. B **85**, 100406(R) (2012).

[13] H. Dixit, J. Hee Lee, J. T. Krogel, S. Okamoto, and V. R. Cooper, Stabilization of weak ferromagnetism by strong magnetic response to epitaxial strain in multiferroic $BiFeO_3$, Sci. Rep. **5**, 12969 (2015).

[14] Z. Chen, Z. Chen, C.-Y. Kuo, Y. Tang, L. R. Dedon, Q. Li, L. Zhang, C. Klewe, Y.-L. Huang, B. Prasad, A. Farhan, M. Yang, J. D. Clarkson, S. Das, S. Manipatruni, A. Tanaka, P. Shafer, E. Arenholz, A. Scholl, Y.-H. Chu, Z. Q. Qiu, Z. Hu, L.-H. Tjeng, R. Ramesh, L.-W. Wang, and L. W. Martin, Complex strain evolution of polar and magnetic order in multiferroic $BiFeO_3$ thin films, Nat. Commun. **9**, 3764 (2018).

[15] S. Kawachi, A. Miyake, T. Ito, S. E. Dissanayake, M. Matsuda, W. Ratcliff, Z. Xu, Y. Zhao, S. Miyahara, N. Furukawa, and M. Tokunaga, Successive field-induced transitions in $BiFeO_3$ around room temperature, Phys. Rev. Mater. **1**, 024408 (2017).

[16] E. R. Callen and H. B. Callen, Static magnetoelastic coupling in cubic crystals, Phys. Rev. **129**, 578 (1963).

[17] E. Callen and H. B. Callen, Magnetostriction, forced magnetostriction, and anomalous thermal expansion in ferromagnets, Phys. Rev. **139**, A455 (1965).

[18] E. Callen, Magnetostriction, J. Appl. Phys. **39**, 519 (1968).

[19] R. Alben and E. Callen, Magnetoelastic spin Hamiltonians: Applications to garnets, Phys. Rev. **186**, 522 (1969).

[20] K. P. Belov, A. K. Zvezdin, and A. M. Kadomtseva, Rare-earth orthoferrites, symmetry and non-Heisenberg exchange, Sov. Sci. Rev. A. Phys. **9**, 117 (1987).

[21] M. Doerr, M. Rotter, and A. Lindbaum, Magnetostriction in rare-earth based antiferromagnets, Adv. Phys. **54**, 1 (2005).

[22] A. M. Kadomtseva, A. K. Zvezdin, Yu. P. Popov, A. P. Pyatakov, and G. P. Vorobev, Space-time parity violation and magnetoelectric interactions in antiferromagnets, JETP Lett. **79**, 571 (2004).

[23] M. Tokunaga, M. Azuma, and Y. Shimakawa, High-field study of strong magnetoelectric coupling in single-domain crystals of $BiFeO_3$, J. Phys. Soc. Jpn. **79**, 064713 (2010).

[24] J. Park, S.-H. Lee, S. Lee, F. Gozzo, H. Kimura, Y. Noda, Y. J. Choi, V. Kiryukhin, S.-W. Cheong, Y. Jo, E. S. Choi, L. Balicas, G. S. Jeon, and J.-G. Park, Magnetoelectric feedback among magnetic order, polarization, and lattice in multiferroic $BiFeO_3$, J. Phys. Soc. Jpn. **80**, 114714 (2011).

[25] M. Tokunaga, M. Akaki, a. Miyake, T. Ito, and H. Kuwahara, High field studies on $BiFeO_3$ single crystals grown by the laser-diode heating floating zone method, J. Magn. Magn. Mater. **383**, 259 (2014).

[26] R. T. Smith, G. D. Achenbach, R. Gerson, and W. J. James, Dielectric properties of solid solutions of $BiFeO_3$ with Pb(Ti, Zr)O_3 at high temperature and high frequency, J. Appl. Phys. **39**, 70 (1968).

[27] J. R. Teague, R. Gerson, and W. J. James, Dielectric hysteresis in single crystal $BiFeO_3$, Solid State Commun. **8**, 1073 (1970).

[28] J. M. Moreau, C. Michel, R. Gerson, and W. J. James, Ferroelectric $BiFeO_3$ x-ray and neutron diffraction study, J. Phys. Chem. Solids **32**, 1315 (1971).

[29] I. Sosnowska, T. Peterlin-Neumaier, and E. Steichele, Spiral magnetic ordering in bismuth ferrite, J. Phys. C: Solid State Phys. **15**, 4835 (1982).

[30] D. Lebeugle, D. Colson, A. Forget, M. Viret, A. M. Bataille, and A. Gukasov, Electric-Field-Induced Spin Flop in $BiFeO_3$ Single Crystals at Room Temperature, Phys. Rev. Lett. **100**, 227602 (2008).

[31] S. Lee, W. Ratcliff, S.-W. Cheong, and V. Kiryukhin, Electric field control of the magnetic state in $BiFeO_3$ single crystals, Appl. Phys. Lett. **92**, 192906 (2008).

[32] M. Ramazanoglu, W. Ratcliff, Y. J. Choi, S. Lee, S.-W. Cheong, and V. Kiryukhin, Temperature-dependent properties of the magnetic order in single-crystal $BiFeO_3$, Phys. Rev. B **83**, 174434 (2011).

[33] J. Herrero-Albillos, G. Catalan, J. A. Rodriguez-Velamazan, M. Viret, D. Colson, and J. F Scott, Neutron diffraction study of the $BiFeO_3$ spin cycloid at low temperature, J. Phys.: Condens. Matter **22**, 256001 (2010).

[34] I. Sosnowska and R. Przeniosło, Low-temperature evolution of the modulated magnetic structure in the ferroelectric antiferromagnet $BiFeO_3$, Phys. Rev. B **84**, 144404 (2011).

[35] S. Bordács, D. G. Farkas, J. S. White, R. Cubitt, L. DeBeer-Schmitt, T. Ito, and I. Kézsmárki, Magnetic Field Control of Cycloidal Domains and Electric Polarization in Multiferroic $BiFeO_3$, Phys. Rev. Lett. **120**, 147203 (2018).

[36] K. Ohoyama, S. Lee, S. Yoshii, Y. Narumi, T. Morioka, H. Nojiri, G. S. Jeon, S.-W. Cheong, and J.-G. Park, High field neutron diffraction studies on metamagnetic transition of multiferroic $BiFeO_3$, J. Phys. Soc. Jpn. **80**, 125001 (2011).

[37] Y. F. Popov, A. K. Zvezdin, G. P. Vorob'ev, A. M. Kadomtseva, V. A. Murashev, and D. N. Rakov, Linear magnetoelectric effect and phase transitions in bismuth ferrite, $BiFeO_3$, JETP Lett. **57**, 69 (1993).

[38] C. Michel, J.-M. Moreau, G. D. Achenbach, R. Gerson, and W. J. James, The atomic structure of $BiFeO_3$, Solid State Commun. **7**, 701 (1969).

[39] F. Kubel and H. Schmid, Structure of a ferroelectric and ferroelastic monodomain crystal of the perovskite $BiFeO_3$, Acta Crystallogr. Sect. B **46**, 698 (1990).

[40] A. Palewicz, R. Przeniosło, I. Sosnowska, and A. W. Hewat, Atomic displacements in $BiFeO_3$ as a function of temperature: Neutron diffraction study, Acta Crystallogr. B **63**, 537 (2007).

[41] A. Palewicz, I. Sosnowska, R. Przenioslo, and A. W. Hewat, $BiFeO_3$ crystal structure at low temperatures, Acta Phys. Pol. **117**, 296 (2010).

[42] I. Sosnowska, R. Przeniosło, A. Palewicz, D. Wardeckiand, and A. Fitch, Monoclinic deformation of crystal lattice of bulk α-$BiFeO_3$: High resolution synchrotron radiation studies, J. Phys. Soc. Jpn. **81**, 044604 (2012).

[43] H. Wang, C. Yang, J. Lu, M. Wu, J. Su, K. Li, J. Zhang, G. Li, T. Jin, T. Kamiyama, F. Liao, J. Lin, and Y. Wu, On the structure of α-$BiFeO_3$, Inorg. Chem. **52**, 2388 (2013).

[44] J. Jeong, E. A. Goremychkin, T. Guidi, K. Nakajima, G. S. Jeon, S.-A. Kim, S. Furukawa, Y. B. Kim, S. Lee, V. Kiryukhin, S.-W. Cheong, and J.-G. Park, Spin Wave Measurements Over the Full Brillouin Zone of Multiferroic $BiFeO_3$, Phys. Rev. Lett. **108**, 077202 (2012).

[45] M. Matsuda, R. S. Fishman, T. Hong, C. H. Lee, T. Ushiyama, Y. Yanagisawa, Y. Tomioka, and T. Ito, Magnetic Dispersion and Anisotropy in Multiferroic $BiFeO_3$, Phys. Rev. Lett. **109**, 067205 (2012).

[46] Z. Xu, J. Wen, T. Berlijn, P. M. Gehring, C. Stock, M. B. Stone, W. Ku, G. Gu, S. M. Shapiro, R. J. Birgeneau, and G. Xu, Thermal evolution of the full three-dimensional magnetic excitations in the multiferroic $BiFeO_3$, Phys. Rev. B **86**, 174419 (2012).

[47] J. Jeong, M. D. Le, P. Bourges, S. Petit, S. Furukawa, S.-A. Kim, S. Lee, S.-W. Cheong, and J.-G. Park, Temperature-Dependent Interplay of Dzyaloshinskii-Moriya Interaction and

Single-Ion Anisotropy in Multiferroic $BiFeO_3$, Phys. Rev. Lett. **113**, 107202 (2014).

[48] M. Cazayous, Y. Gallais, A. Sacuto, R. de Sousa, D. Lebeugle, and D. Colson, Possible Observation of Cycloidal Electromagnons in $BiFeO_3$, Phys. Rev. Lett. **101**, 037601 (2008).

[49] P. Rovillain, R. de Sousa, Y. Gallais, A. Sacuto, M. A. Méasson, D. Colson, A. Forget, M. M. Bibes, A. Barthélémy, and M. Cazayous, Electric-field control of spin waves at room temperature in multiferroic $BiFeO_3$, Nat. Mater. **9**, 975 (2010).

[50] B. Ruette, S. Zvyagin, A. P. Pyatakov, A. Bush, J. F. Li, V. I. Belotelov, A. K. Zvezdin, and D. Viehland, Magnetic-field-induced phase transition in $BiFeO_3$ observed by high-field electron spin resonance: Cycloidal to homogeneous spin order, Phys. Rev. B **69**, 064114 (2004).

[51] D. Talbayev, S. A. Trugman, S. Lee, H. T. Yi, S.-W. Cheong, and A. J. Taylor, Long-wavelength magnetic and magnetoelectric excitations in the ferroelectric antiferromagnet $BiFeO_3$, Phys. Rev. B **83**, 094403 (2011).

[52] U. Nagel, R. S. Fishman, T. Katuwal, H. Engelkamp, D. Talbayev, H. T. Yi, S.-W. Cheong, and T. Rõõm, Terahertz Spectroscopy of Spin Waves in Multiferroic $BiFeO_3$ in High Magnetic Fields, Phys. Rev. Lett. **110**, 257201 (2013).

[53] I. Kézsmárki, U. Nagel, S. Bordács, R. S. Fishman, J. H. Lee, H. T. Yi, S.-W. Cheong, and T. Rõõm, Optical Diode Effect at Spin-Wave Excitations of the Room-Temperature Multiferroic $BiFeO_3$, Phys. Rev. Lett. **115**, 127203 (2015).

[54] R. S. Fishman, J. H. Lee, S. Bordács, I. Kézsmárki, U. Nagel, and T. Rõõm, Spin-induced polarizations and nonreciprocal directional dichroism of the room-temperature multiferroic $BiFeO_3$, Phys. Rev. B **92**, 094422 (2015).

[55] T. Ito, T. Ushiyama, Y. Yanagisawa, R. Kumai, and Y. Tomioka, Growth of highly insulating bulk single crystals of multiferroic $BiFeO_3$ and their inherent internal strains in the domain-switching process, Cryst. Growth Des. **11**, 5139 (2011).

[56] See Supplemental Material at http://link.aps.org/supplemental/10.1103/PhysRevB.102.214410 for a derivation of the possible magnetoelastic coupling terms consistent with monoclinic symmetry.

[57] R. S. Fishman, The microscopic model of $BiFeO_3$, Physica B **536**, 115 (2018).

[58] R. S. Fishman, Pinning, rotation, and metastability of $BiFeO_3$ cycloidal domains in a magnetic field, Phys. Rev. B **97**, 014405 (2018).

[59] I. Sosnowska and A. Zvezdin, Origin of long period magnetic ordering in $BiFeO_3$, J. Magn. Magn. Mater. **140-144**, 167 (1995).

[60] A. P. Pyatakov and A. K. Zvezdin, Flexomagnetoelectric interaction in multiferroics, Eur. Phys. J. B **71**, 419 (2009).

[61] Rhombohedral distortion of a cube, elongation along the body diagonal, introduces two different J_2 couplings. The difference between the two is not taken into account because the spin-wave frequencies do not depend on J_2 at $\mathbf{q} = 0$.

[62] R. S. Fishman, J. A. Fernandez-Baca, and T. Rõõm, *Spin-Wave Theory and its Applications to Neutron Scattering and THz Spectroscopy* (IOP Concise Physics, Morgan and Claypool Publishers, San Rafael, CA, 2018).

[63] M. Tokunaga, M. Akaki, H. Kuwahara, T. Ito, A. Matsuo, and K. Kindo, Magnetoelectric effects in mono-domain crystals of $BiFeO_3$, JPS Conf. Proc. **3**, 014038 (2014).

[64] M. Ramazanoglu, M. Laver, W. Ratcliff, S. M. Watson, W. C. Chen, A. Jackson, K. Kothapalli, S. Lee, S.-W. Cheong, and V. Kiryukhin, Local Weak Ferromagnetism in Single-Crystalline Ferroelectric $BiFeO_3$, Phys. Rev. Lett. **107**, 207206 (2011).

[65] A. V. Zalesskii, A. K. Zvezdin, A. A. Frolov, and A. A. Bush, ^{57} Fe NMR study of a spatially modulated magnetic structure in $BiFeO_3$, J. Exp. Theor. Phys. Lett. **71**, 465 (2000).

[66] A. V. Zalesskii, A. A. Frolov, A. K. Zvezdin, A. A. Gippius, E. N. Morozova, D. F. Khozeevc, A. S. Bush, and V. S. Pokatilov, Effect of spatial spin modulation on the relaxation and NMR frequencies of ^{57}Fe nuclei in a ferroelectric antiferromagnet $BiFeO_3$, J. Exp. Theor. Phys. **95**, 101 (2002).

[67] R. S. Fishman, J. T. Haraldsen, N. Furukawa, and S. Miyahara, Spin state and spectroscopic modes of multiferroic $BiFeO_3$, Phys. Rev. B **87**, 134416 (2013).

[68] R. de Sousa, M. Allen, and M. Cazayous, Theory of Spin-Orbit Enhanced Electric-Field Control of Magnetism in Multiferroic $BiFeO_3$, Phys. Rev. Lett. **110**, 267202 (2013).

[69] Z. V. Gareeva, A. F. Popkov, S. V. Soloviov, and A. K. Zvezdin, Field-induced phase transitions and phase diagrams in $BiFeO_3$-like multiferroics, Phys. Rev. B **87**, 214413 (2013).

[70] M. Matsuda, S. E. Dissanayake, T. Hong, Y. Ozaki, T. Ito, M. Tokunaga, X. Z. Liu, M. Bartkowiak, and O. Prokhnenko, Magnetic field induced antiferromagnetic cone structure in multiferroic $BiFeO_3$, Phys. Rev. Mater. **4**, 034412 (2020).

[71] We could have fixed D_2 using the measured M_0, thereby reducing the number of fitting parameters from five to four. However, we elected to leave D_2 free for two reasons. First, M_0 is not known very accurately from experiments. Second, the resulting theoretical value for M_0 can be used to test the model.

[72] M. Tokunaga, M. Azuma, and Y. Shimakawa, High-field study of multiferroic $BiFeO_3$, J. Phys.: Conf. Ser. **200**, 012206 (2010).

[73] M. Tokunaga, M. Akaki, T. Ito, S. Miyahara, A. Miyake, H. Kuwahara, and N. Furukawa, Magnetic control of transverse electric polarization in $BiFeO_3$, Nat. Commun. **6**, 5878 (2015).

[74] S. Kawachi, S. Miyahara, T. Ito, A. Miyake, N. Furukawa, Jun-ichi Yamaura, and M. Tokunaga, Direct coupling of ferromagnetic moment and ferroelectric polarization in $BiFeO_3$, Phys. Rev. B **100**, 140412(R) (2019).

[75] C. Jia, S. Onoda, N. Nagaosa, and J. H. Han, Bond electronic polarization induced by spin, Phys. Rev. B **74**, 224444 (2006).

[76] http://energy.gov/downloads/doe-public-access-plan.